https://dx.doi.org/10.22161/ijaems.63.1 ISSN: 2454-1311

# Sensor-less DC-Voltage Control for Grid-Connected Inverters

Quang-Tho Tran*, Quang-Hieu Nguyen

FEEE, HCMC University of Technology and Education, HCM city, Vietnam
*: Corresponding author

***Abstract***— *Three-phase grid-connected inverters using solar energy are applied very popular with large capacity. These inverters usually have input power sources in the direct current (DC) that varies according to the weather conditions. The DC voltage often needs to boost up the higher voltage level to be in accordance with the output voltage of inverters. Then, the output voltage of the DC/DC boost converter is in the form of DC voltage. In order to measure this DC value in the two-stage inverters, the existing methods usually use isolated voltage sensors. This paper presents a strategy for estimating the DC voltage value of inverters without using sensors in order to reduce cost and volume for inverters. The proposed method contributes to decreasing the price of inverters while ensuring the power quality of inverter outputs. The simulated results on MATLAB/Simulink have validated the performance of the presented solution.*

***Keywords***— ***Current harmonics, DC voltage controllers, grid-connected inverters, sensor-less DC-link voltage.***

## I. INTRODUCTION

Renewable energies such as wind powers and solar powers are increasingly used due to its sustainability and environment. Because of the heavy dependence on weather conditions, these renewable energy sources have an unstable characteristic. Therefore, in order to become the high-quality, efficient power sources, these energies need to be connected to the grid through power semiconductor grid-connected inverters [1]–[3]. In operation, grid-connected inverters must meet the required power quality standards [4], [5]. Due to the output of the solar panels or the wind turbine generators is usually in form of direct-current (DC) and its capacity and voltage change according to weather conditions. Therefore, two-stage or single-stage grid-connected inverters with maximum power point detection function often have to use a DC voltage sensor to control this DC-link voltage value [6], [7]. The use of Hall sensors to isolate DC voltage for ensuring the safety of control circuits has increased the cost and space of the device.

The study of removing this sensor will contribute to reducing space and hardware, which will reduce device costs. However, this makes it difficult to control the quality of the output power, since the output current harmonics depend on the DC voltage value. Therefore, the accurate estimation of the DC voltage value without using the sensor has become a challenge. The control of DC-link voltage in grid-connected inverters plays an important role in system stability [8]–[10]. There have been solutions recommended to solve this problem. The work published in [11] introduced a control method without DC voltage sensor by estimating this value. However, this method has only applied for three-phase rectifiers. The method in [12] using the output current and the grid voltage to detect the DC-link voltage is only used for inverters with the fixed DC voltage. Another work in [13] has proposed a diagram without voltage sensor and removed the voltage control loop. However, the authors of this work have used neural networks to replace for the voltage control loop and only applied for the single-phase grid-connected inverters. This makes it difficult for large-scale inverter applications. The technique without DC voltage sensor in [14] has used the grid voltage to estimate the reference DC voltage. This may be inappropriate when the grid voltage changes and lead to the change of the estimated DC voltage. Meanwhile, the output voltage of DC-DC converter is still fixed.

This paper proposes a method for controlling the DC-link voltage without using a voltage sensor to reduce device cost and space regardless of the voltage drop of the converter. The value of the reference current for the inverter is estimated based on the voltage at the maximum power point of the solar modules. Section 2 in the paper introduces a method for controlling three-phase grid-

*https://dx.doi.org/10.22161/ijaems.63.1* *ISSN: 2454-1311*

connected photovoltaic inverters using the DC voltage sensor. The details of the proposed strategy without the DC voltage sensor are presented in Section 3. The simulation results are showed and discussed in Section 4. The conclusions in Section 5 show the performance of the proposed technique compared with that of the method using the sensor.

## II. CONTROL OF DC-LINK VOLTAGE

The structure of a two-stage grid-connected inverter system using solar energy is shown in Fig. 1. The block of MPPT is responsible for detecting the maximum power point using the INC algorithm [15]. The outputs of this block are a PWM pulse for the DC/DC boost converter and a maximum power $P_{MPPT}$ of the solar modules. The value of $P_{MPPT}$ is used for calculating the reference current $I_{d\_ref}$, that determines the amount of active power injected into the grid.

In Fig. 1, the phase-locked loop (PLL) functions to detect the magnitude $V_{max}$, frequency f, and angle θ of the grid voltage. This helps the inverter synchronize with the power network while it generates powers into the grid.

The control principle diagram of an inverter system is shown in Fig. 2. In the normal operation conditions, the inverter does not need to generate the reactive power Q into the grid. Thus, the reference reactive current $I_{q\_ref}$ is zero. The reference DC-link voltage $V_{ref}$ is defined by the modulation index and the voltage magnitude as (1).

$$V_{ref} = \frac{2*V_{max}}{m} \quad (1)$$

Where m is the modulation index, and $V_{max}$ is the voltage magnitude of the grid.

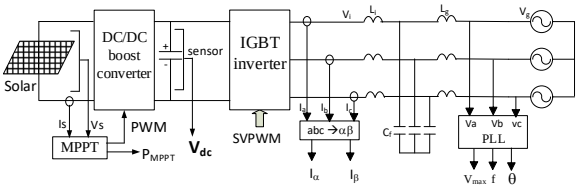


*Fig. 1: Principle diagram of grid-connected photovoltaic inverter system*

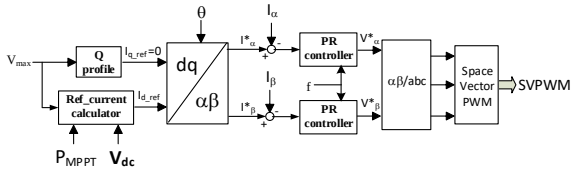


*Fig. 2: Control diagram of grid-connected inverter*

The reference current calculation block of $I_{d\text{-}ref}$ is shown in Fig. 3 and calculated as (2). This current will define the active power injected into the grid.

$$I_{d\_ref} = \frac{P_{MPPT}}{V_{max}} + \Delta I_{d\_ref} \quad (2)$$

Where $\Delta I_{d\text{-}ref}$ depends on the DC-link voltage regulation via a PI controller.

$$\Delta I_{d\_ref} = (V_{dc} - V_{ref}) * \left( K_{p-PI} + \frac{K_{i-PI}}{s} \right) = error * \left( K_{p-PI} + \frac{K_{i-PI}}{s} \right) \quad (3)$$

Where the error is the difference between the reference DC voltage value and the one measured by the sensor. Thus, it always needs a DC-link voltage sensor in order to calculate the reference current for the inverter.

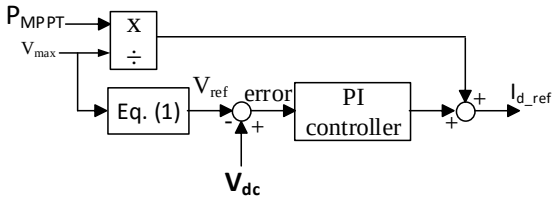


*Fig. 3: Reference current calculation block when using voltage sensor*

The DC/DC boost converter is shown in Fig. 4 and used to boost from the panel voltage $V_s$ up to the reference DC-link voltage $V_{dc}$.

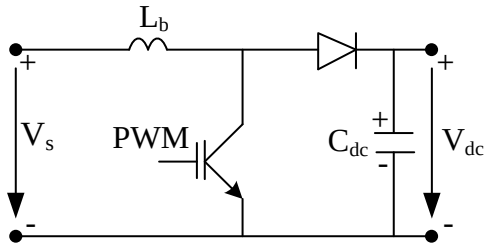


*Fig. 4: Boost converter principle diagram*

## III. THE PROPOSED STRATEGY

As mentioned above, there is always a sensor to measure DC-link voltage of the inverter. In the proposed technique, the DC-link voltage value is estimated by using the outputs of the MPPT block.

Basing on the blocks MPPT and DC/DC boost converter, the DC-link voltage value is estimated as (4).

*https://dx.doi.org/10.22161/ijaems.63.1* *ISSN: 2454-1311*

$$V_{dc-estimated} = \frac{V_{solar}}{1 - D_{PWM}} \quad (4)$$

Where the voltage $V_{solar}$ and the duty $D_{PWM}$ are the voltage value and the pulse-width-modulation of the solar panels at the maximum power point, respectively. The estimation principle diagram is also described in Fig. 5. Where $V_{dc\text{-}estimated}$ is the estimated DC-link voltage value. This method has not been affected by the voltage drop of the boost devices.

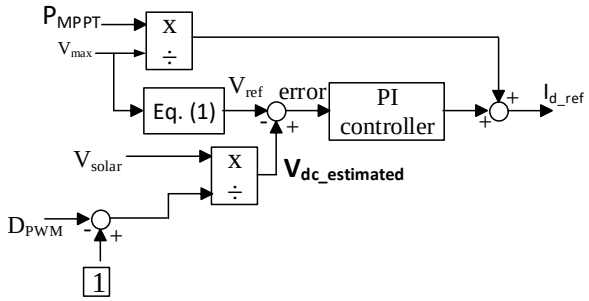


*Fig. 5: The proposed reference current calculation.*

## IV. SIMULATION RESULTS

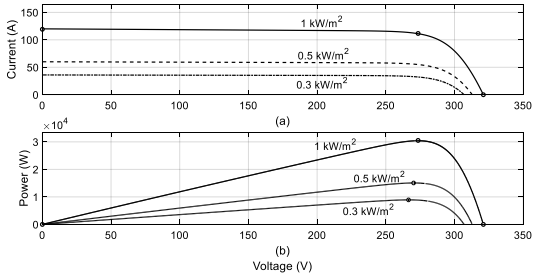


*Fig. 6: V-A and V-W curves of the solar panels*

The system model of this paper has used 90 solar panels from SUNPOWER, SPR-305E-WHT-D. Each panel has a peak power 305.226 Wp. All panels are 20 parallel-connected strings and each string consists of 5 series-connected panels. The total power of the system is 30.522kWp. The solar panel characteristics of the system in Fig. 6 show the voltage at the maximum power point about 270VDC. Then, the converter in Fig. 4 boosts this voltage value up to about 730VDC by the duty $D_{PWM}$.

In order to be appropriate to actual changes of irradiance conditions, there are 3 intervals of time selected in the same condition of 25°C to test 3 different irradiance levels, respectively. In the first interval of time, 0-0.4s, irradiance level is 1000W/m$^2$ (1pu). In the second interval, 0.4-0.7s, the irradiance is 500W/m$^2$ (0.5pu), and 300W/m$^2$ (0.3pu) is the irradiance level for the last interval 0.7-1s. The system parameters are showed in Table 1.

*Table 1: System parameters*

| Description | Symbol | Value |
|---|---|---|
| Total peak power of solar panels | Solar | 30.522 Wp |
| Grid voltage | $V_g$ | 3x380 V |
| Grid frequency | f | 50 Hz |
| DC capacitor | $C_{dc}$ | 1000 µF |
| Filter inductor | $L_i$ | 7.5 mH |
| Filter capacitor | $C_f$ | 7.5 µF |
| Modulation index | m | 0.8 |
| DC voltage regulator coefficients | $K_p$-PI<br>$K_i$-PI | 0.2<br>2.5 |
| Current controller coefficients | $K_p$-PR<br>$K_i$-PR | 110.37<br>304.2 |
| DC/DC booster switching frequency | PWM | 2 kHz |
| Inverter switching frequency | SVPWM | 5 kHz |

### 4.1. THE METHOD OF USING VOLTAGE SENSOR

The simulation results of the method using sensor are showed in Figs. 7-13. The output current waveforms in Ampere and total harmonic distortion (THD) are shown in Figs. 11-13 and measured at the moments 0.38s, 0.68s, and 0.98s, respectively.

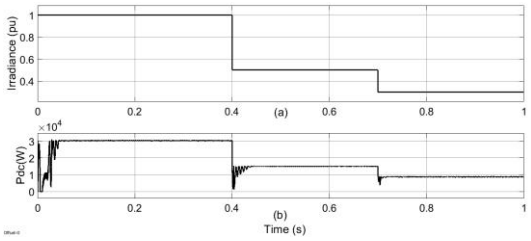


*Fig. 7: Maximum power levels of the solar panels for three different irradiances*

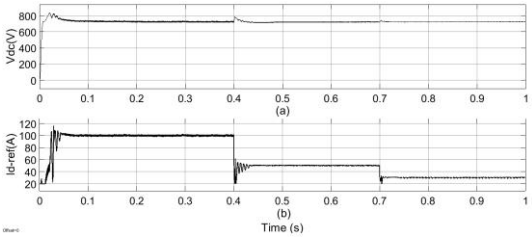


*Fig. 8: DC-link voltage and reference current $I_{\_dref}$*

*https://dx.doi.org/10.22161/ijaems.63.1* *ISSN: 2454-1311*

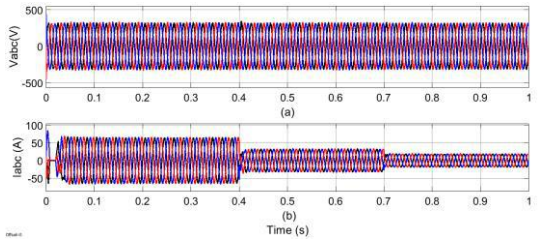


*Fig. 9: Output three-phase voltages and currents*

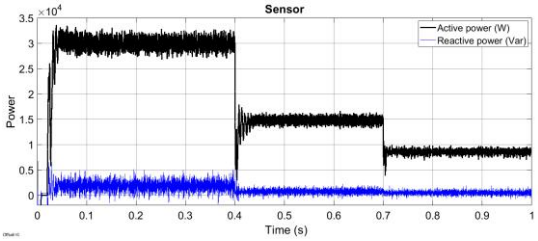


*Fig. 10: Active and reactive powers*

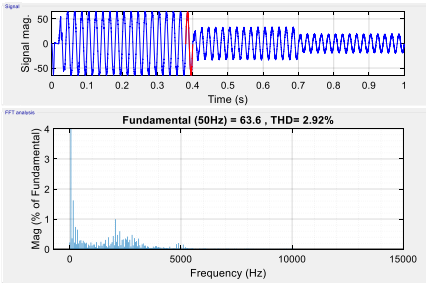


*Fig. 11: Current THD of phase A measured in the first interval*

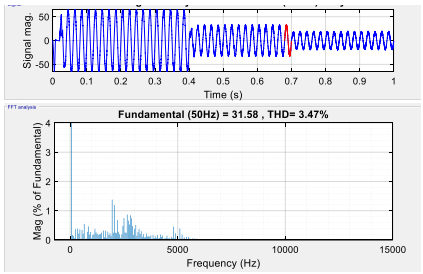


*Fig. 12: Current THD of phase A in the second interval*

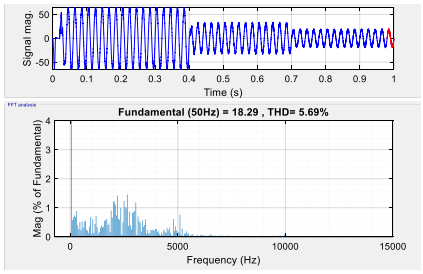


*Fig. 13: Current THD of phase A in the final interval*

## 4.2. THE PROPOSED METHOD

The simulation results of the proposed method are shown in Figs. 14-21.

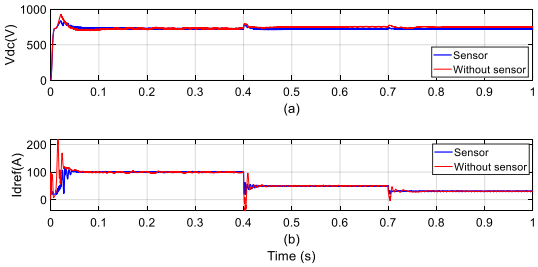


*Fig. 14: Responses of the estimated DC voltage and reference current*

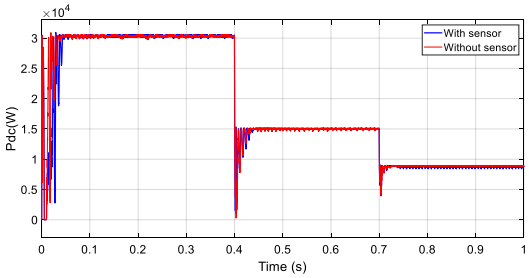


*Fig. 15: DC side power responses*

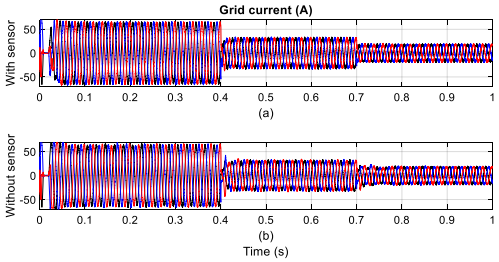


*Fig. 16: Inverter output currents*

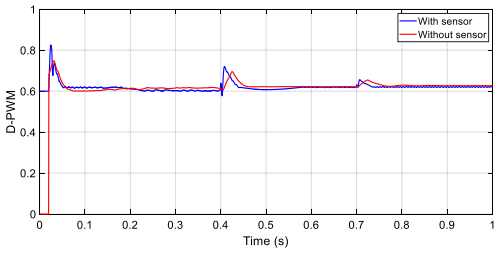


*Fig. 17: $D_{PWM}$ responses of the simulation cases*

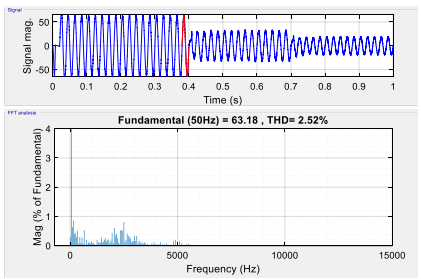


*Fig. 18: Current THD of phase A in the first interval*

*https://dx.doi.org/10.22161/ijaems.63.1* *ISSN: 2454-1311*

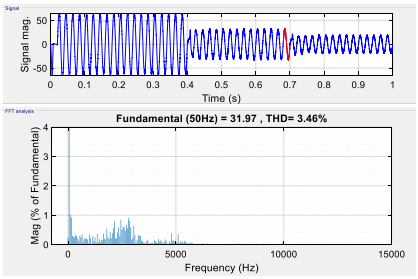


*Fig. 19: Current THD of phase A in the second interval*

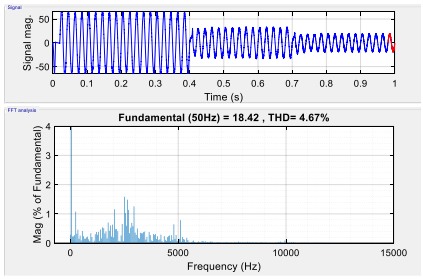


*Fig. 20: Current THD of phase A in the final interval*

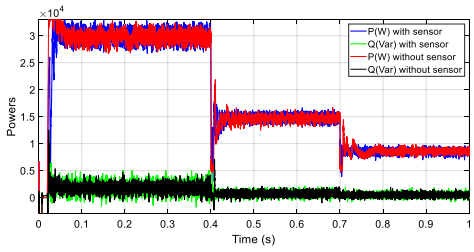


*Fig. 21: Active power responses injected into the grid*

4.3. DISCUSSIONS

The results in Figs. 7-13 showed the overshoot and steady-state error of the DC voltage for the method using voltage sensor are relatively small. However, the output current THD is higher than that of the proposed method causes the output power responses in Fig. 10 to have the higher steady-state errors in Fig. 21. The current THD values of the method using sensor in Figs. 11-13 are measured at the final sinewave period in the intervals of time, respectively. The current THD results for the 2 cases are also showed in Table 2.

*Table 2: Fundamental grid current magnitudes and total harmonic distortions*

| Intervals | | 0-0.4s | 0.4-0.7s | 0.7-1s |
|---|---|---|---|---|
| Sensor | Ip (A) | 63.6 | 31.58 | 18.29 |
| | THD (%) | **2.92** | **3.47** | **5.69** |
| Proposed | Ip (A) | 63.18 | 31.97 | 18.42 |
| | THD (%) | **2.52** | **3.46** | **4.67** |

Although the steady state error and the overshoot of DC-link voltage for the proposed method in Fig. 14(a) are slightly higher than those of the method using sensor and make the reference current in Fig. 14(b) and the DC power in Fig. 15 be also slightly higher, these do not cause over-current for the inverter in Fig. 16(b).

The DC-link voltage responses for the two cases are also showed in Fig. 14(a). The voltage value of the proposed method is the signal in the red. This value is slightly higher than that of the method using sensor. Because its duty $D_{PWM}$ in Fig. 17 is also a bit higher than that of the method using sensor. This also makes the current magnitude injected into the grid a bit higher than that of the method using sensor. As a result, the current harmonics of the proposed method are slightly lower than that of the method using sensor. The current waveforms (unit of Ampere) and THD (%) of the phase A are shown in Figs. 18-20 using the FFT of Matlab/Simulink. These values are slightly lower than those of the method using sensor in Figs. 11-13 and shown in Table 2. The lower current harmonics of the proposed method also contribute to reducing the steady state error of the active power injected into the grid in Fig. 21. In the interval of 0.7s-1s, the actual voltage value is bit higher than the estimated one due to the voltage loss of the filter. However, the power quality of the proposed method is also similar to that of the method using sensor.

## V. CONCLUSION

This paper has proposed a method for estimating the DC-link voltage of the grid-connected inverters to remove the DC voltage sensor. The estimation is based on the DC maximum power and the PWM duty of the DC/DC booster regardless of the voltage drop on the converter devices. The simulation results showed the power quality of the proposed method is similar to that of the method using sensor. This has validated the performance of the proposed method. The study of reducing hardware space and device costs for grid-connected inverters also helps the manufacturers increase the competition.

## ACKNOWLEDGEMENTS

I would like to acknowledge the support of the Renewable energy and Power systems Lab C201 from HCM UTE-Vietnam.

*https://dx.doi.org/10.22161/ijaems.63.1* *ISSN: 2454-1311*

## REFERENCES


[1] Z. Chen, J. M. Guerrero, F. Blaabjerg, and S. Member, "A Review of the State of the Art of Power Electronics for Wind Turbines," *IEEE Trans. Power Electron.*, vol. 24, no. 8, pp. 1859–1875, 2009.

[2] R. Teodorescu, M. Liserre, and P. Rodriguez, *Grid Converters for Photovoltaic and Wind Power Systems*. 2011.

[3] K. Zeb *et al.*, "A comprehensive review on inverter topologies and control strategies for grid connected photovoltaic system," vol. 94, no. June, pp. 1120–1141, 2018.

[4] IEEE Standard, "IEEE Application Guide for IEEE Std 1547(TM), IEEE Standard for Interconnecting Distributed Resources with Electric Power Systems," *IEEE Std 1547.2-2008*, no. April, pp. 1–217, 2009.

[5] A. Anzalchi and A. Sarwat, "Overview of technical specifications for grid-connected photovoltaic systems," *Energy Convers. Manag.*, vol. 152, no. September, pp. 312–327, 2017.

[6] A. Rajashekar and S. Swathi, "Grid Interconnection of Renewable Energy Sources with Power- Quality Improvement Features at the Distribution Level," *IEEE Trans. Power Deliv.*, vol. 26, no. 1, pp. 307–315, 2011.

[7] H. D. Tafti, A. I. Maswood, G. Konstantinou, J. Pou, and F. Blaabjerg, "A general constant power generation algorithm for photovoltaic systems," *IEEE Trans. Power Electron.*, vol. 33, no. 5, pp. 4088–4101, 2018.

[8] A. M. A. Haidar and N. Julai, "Energy for Sustainable Development An improved scheme for enhancing the ride-through capability of grid-connected photovoltaic systems towards meeting the recent grid codes requirements," *Energy Sustain. Dev.*, vol. 50, pp. 38–49, 2019.

[9] A. Q. Al-Shetwi, M. Z. Sujod, and F. Blaabjerg, "Low voltage ride-through capability control for single-stage inverter-based grid-connected photovoltaic power plant," *Sol. Energy*, vol. 159, pp. 665–681, 2018.

[10] A. Turksoy, Y. Hames, A. Teke, and M. Barghi, "A novel adaptive switching method to reduce DC-Link capacitor ripple in PV based grid-connected inverter," *Sol. Energy*, vol. 173, no. February, pp. 702–714, 2018.

[11] A. Mallik, S. Member, A. Khaligh, and S. Member, "DC Link Voltage Sensorless Control of a Three-Phase Boost Power Factor Correction Rectifier," in *2016 IEEE Transportation Electrification Conference and Expo (ITEC)*, 2016, pp. 1–6.

[12] Z. Wang, L. Chang, and M. Mao, "Dc voltage sensorless control method for three-phase grid-connected inverters," *IET Power Electron.*, vol. 3, no. 4, pp. 552–558, 2010.

[13] N. E. Zakzouk, A. K. Abdelsalam, and A. A. Helal, "PV Single Phase Grid Connected Converter : DC - link Voltage Sensorless Prospective," *IEEE J. Emerg. Sel. Top. Power Electron.*, vol. 5, no. 1, pp. 526–546, 2017.

[14] V. Kumar and M. Singh, "Sensorless DC-link control approach for three-phase grid integrated PV system," *Electr. Power Energy Syst.*, vol. 112, pp. 309–318, 2019.

[15] O. Wasynczuk, "Dynamic behavior of a class of photovoltaic power systems," *," IEEE Power Eng. Rev.*, no. September, pp. 36–37, 1983.